Behavior of a Thermotropic Nematic Liquid Crystal Confined to Controlled Pore Glasses as Studied by ^{129}Xe NMR Spectroscopy

Pekka Tallavaara, Ville-Veikko Telkki, and Jukka Jokisaari*

NMR Research Group, Department of Physical Sciences, University of Oulu, P.O. Box 3000, FIN-90014 University of Oulu, Finland

Received: July 5, 2006; In Final Form: August 17, 2006

The behavior of nematic liquid crystal (LC) Merck Phase 4 confined to controlled pore glass (CPG) materials was investigated using ^{129}Xe nuclear magnetic resonance (NMR) spectroscopy of xenon gas dissolved in the LC. The average pore diameters of the materials varied from 81 to 2917 Å, and the measurements were carried out within a wide temperature range (∼185−370 K). The spectra contain lots of information about the effect of confinement on the phase of the LC. The theoretical model of shielding of noble gases dissolved in liquid crystals on the basis of pairwise additivity approximation was applied to the analysis of the spectra. When pore diameter is small, smaller than ∼150 Å, xenon experiences on average an isotropic environment inside the pore, and no nematic−isotropic phase transition is observed. When the size is larger than ∼150 Å, nematic phase is observed, and the LC molecules are oriented along pore axis. The orientational order parameter of the LC, *S*, increases with increasing pore size. In the largest pores, the orientation of the molecules deviates from the pore axis direction to magnetic field direction, which implies that the size of the pores (∼3000 Å) is close to magnetic coherence length. The decrease of magnetic coherence length with increasing temperature is clearly seen from the spectra. When the sample is cooled rapidly by immersing it in liquid nitrogen, xenon atoms do not squeeze out from the solid, as they do during gradual freezing, but they are occluded inside the solid lattice, and their chemical shift is very sensitive to crystal structure. This makes it possible to study the effect of confinement on the solid phases. According to the measured ^{129}Xe NMR spectra, possibly three different solid phases are observed from bulk liquid crystal in the used temperature region. The same is also seen from the samples containing larger pores (pore size larger than ∼500 Å), and the solid−solid phase-transition temperatures are the same. However, no first-order solid−solid phase transitions are observed from the smaller pores. Melting point depression, that is, the depression of solid-nematic transition temperature observed from the pores as compared with that in bulk LC, is seen to be very sensitive to the pore size, and it can be used for the determination of pore size of an unknown material.

Introduction

Liquid crystals (LCs) are scientifically fascinating because of their distinctive characteristic as an intermediate phase between liquid and solid. They are also objects of large industrial interest; they are used in LC displays, electrooptic devices, polymer-dispersed liquid crystal (PDLC) light shutters, and so forth. In many applications, LCs are confined to small volumes, and this changes their optical, electrical, and magnetic anisotropic properties as well as their behavior in phase transitions. For the optimal use of LCs in the applications, it is important to systematically study those effects. One way to do this is to absorb LCs inside the porous materials with well-known characteristics.

The properties of LCs confined to large variety of porous materials have been studied using numerous techniques[1] such as light[2] and neutron scattering,[3] Raman spectroscopy,[4] differential scanning calorimetry,[5] magnetic birefringence,[6] evanescent-wave-ellipsometry,[7] small-angle X-ray scattering,[8] and nuclear magnetic resonance (NMR) spectroscopy.[9−14] NMR is especially suitable for investigation of LCs because of the sensitivity of the NMR spectrum to molecular orientational order, director configurations, and molecular dynamics. Because it is a relatively insensitive method, investigation of effects of a single, small surface on the behavior of LCs is practically impossible to carry out. In porous media, however, the total surface area of the walls of the pores is usually very large, even hundreds of square meters per gram, which makes NMR studies conceivable. Usually in NMR experiments, LC molecules are isotopically labeled in such a way that one or more of the hydrogens in the molecules are replaced by deuterium. By measuring deuterium NMR spectrum from this kind of a sample, it is possible to get accurate orientational information.

In the present work, Merck Phase 4 LC (from here on referred to as Phase 4) eutectic mixture of *p*-methoxy-*p*′-butylazoxybenzenes was confined to five controlled pore glass (CPG) materials with nominal pore diameters varying from 81 to 2917 Å. CPG materials contain randomly connected networks of pores with relatively narrow pore size distribution. The behavior of Phase 4 in the confinement was studied by ^{129}Xe NMR of xenon gas dissolved into the LC because the chemical shift of ^{129}Xe isotope (spin $I = {}^1/_2$) is extremely sensitive to the changes of its local environment, and its relative receptivity is much larger than that of the other noble gas isotopes.[15] In addition, no isotope labeling of LC molecule is needed.

Xenon NMR has been used earlier to study an LC confined to parallel, straight cylindrical cavities,[9] but, to our knowledge,

* Author to whom correspondence should be addressed. Tel.: +35885531308 or +358405956146 (mobile); fax: +35885531287; e-mail: Jukka.Jokisaari@oulu.fi.

10.1021/jp064222g CCC: $33.50
Published on Web 10/04/2006

this is the first study in porous networks with randomly oriented and connected pores.

The measurements were performed within a wide temperature range, covering solid, nematic, and isotropic phases. Special emphasis was put on the explanation of the phenomena observed in the nematic range, and a model of nuclear magnetic shielding of dissolved noble gases on the basis of pairwise additivity approximation[16] was used in the analysis. In addition, the influence of pore size on the phase-transition temperatures has been studied. All the results are compared with the spectra of xenon dissolved in the bulk LC.

Isotropic-to-nematic phase transition of thermotropic LC is accompanied by the build-up of long-range orientational order of the molecules. In the isotropic phase, there are still small nematic-like domains where LC molecules are parallel to each other, but the orientations of successive domains do not correlate. According to Landau approximation, the nematic coherence length ξ_N representing the size of the regions can be defined through equation[17]

$$\xi_N = l_0\left(\frac{T^*}{T - T^*}\right)^{1/2} \quad (1)$$

where l_0 is molecular length. T^* is the temperature when the correlation length becomes infinite, and it is typically $\sim$1 K smaller than the nematic−isotropic phase-transition temperature T_{NI}. T^* determines also the lowest temperature down to which one can supercool the isotropic phase. Because the molecular length of Phase 4 LC molecule is about 20 Å, it can be estimated that ξ_N is about 370 Å at 1 K above T^*, and it decreases to 120 Å when temperature is 10 K above T^*.

In the present system, there are two main factors that influence the orientation of molecules in nematic phase: surfaces of the pores and external magnetic field. Bare silica surfaces, such as in the case of CPG materials used in this work, tend to orientate LC molecules along the surfaces. On the other hand, the external magnetic field tends to orientate the molecules parallel with the field, because the anisotropy of diamagnetic susceptibility of Phase 4 is positive. These factors are competing with each other. For instance, near a smooth surface, the orientation of LC molecules is completely determined by the interaction between the molecules and the surface. However, the strength of these interactions diminishes with increasing distance, and sufficiently far from the surface the nematic LCs orientate parallel with (or perpendicular to if the anisotropy of the susceptibility is negative) the external field and behave like bulk LC. Magnetic coherence length, ξ_M, represents this distance, and it is determined through equation[17]

$$\xi_M = \frac{1}{B}\left(\frac{\mu_0 K}{\Delta\chi}\right)^{1/2} \quad (2)$$

Here, B is the external magnetic flux density, μ_0 is permeability of vacuum, K is the elastic constant of the medium, and $\Delta\chi$ is anisotropy of diamagnetic susceptibility. In the magnetic field used in the present study (11.74 T), the magnetic coherence length is about1 μm. It is larger than the diameters of pores (0.0081−0.2917 μm). On the basis of this value of magnetic coherence length, it can be predicted that the magnetic field has negligible role in the orientation and formation of local director distribution inside the cavities in the case of smaller pore sizes. However, because the sizes of the largest pores are of the same order of magnitude with the magnetic coherence length, the external magnetic field may significantly change the orientation of the LC in the middle of the pore. On the other hand, because the size of the CPG particles is about 150 μm, the spaces between the particles are so large that LC outside porous material orientates parallel with magnetic field and behaves like bulk LC.

According to the previous discussion, LC molecules tend to orientate parallel with the pore axis, when the pore size is much smaller than ξ_M. However, randomly connected pores cause defects to the orientation when the lengths of pore segments are about the size of LC molecules. The defects effectively decrease the second-rank orientational order parameter S determined by equation[18]

$$S = \frac{1}{2}\langle 3\cos^2\beta - 1\rangle \quad (3)$$

Here, β is the angle between the director and the long molecular axis. The director represents the average orientation of the molecules and its direction is depicted by a unit vector **n**. Roughness in the surface of a pore may also cause defects to the orientation. However, the atomic force microscopy (AFM) measurements by Kralj et al.[19] revealed that the surface wall of CPG pores is smooth on the length scale larger than the size of a molecule, and therefore it should not significantly disturb the orientational order of nematic phase. Instead, very small pore size (on the order of molecule size) has been found to disturb seriously the nematic orientational order, and the nematic−isotropic transition can be replaced by continuous transition to a glassylike state.[14]

The nuclear magnetic shielding of noble gas atoms dissolved in an LC has been explained using pairwise additivity approximation. According to the model, the average of the shielding tensor element in the direction of the applied magnetic field (Z) can be presented in the form[16]

$$\langle\sigma_{ZZ}\rangle = \rho(T)\Big\{\sigma_0[1 - \beta_1(T - T_0)] + \frac{2}{3}\Delta\sigma_0[1 - \beta_2(T - T_0)]P_2(\cos\theta)S(T)\Big\} \quad (4)$$

where $\rho(T)$ describes the temperature dependence of the density of the LC, coefficients σ_0 and $\Delta\sigma_0$ are the shielding constant and shielding anisotropy (the ^{129}Xe shielding tensor is axially symmetric) per density at the reference temperature T_0, β_1 stands for the temperature dependence of shielding, and β_2 is the temperature dependence of shielding anisotropy. $P_2(\cos\theta) = (^1/_2)(3\cos^2\theta - 1)$ is the second-order Legendre polynomial, where θ is the angle between the LC director **n** and the external magnetic field $\mathbf{B}_0$ and $S(T)$ is the temperature-dependent order parameter.

According to eq 4, the anisotropic part of shielding (or equivalently chemical shift) depends on the orientation of the director of the nematic phase through $P_2(\cos\theta)$ and on the order parameter S. If the magnetic coherence length ξ_M is much larger than pore size, the orientation of the LC is purely determined by the orientation of pore. Because the pores are isotropically oriented in the sample, $P_2(\cos\theta)$ dependence of the anisotropic part is expected to produce a perfect chemical shift anisotropy (CSA) powder pattern line shape. The distortion of nematic order in small pores may lead to reduced value of S, which means that the powder pattern is still observed, but the span of the signal is smaller. In the extreme case, the nematic order does not build up at all. Thus, S is zero and isotropic line shape is observed from the pore.

When the pore size is on the same order of magnitude with ξ_M, the interactions with both the magnetic field and with the

pore walls tend to orientate LC molecules to the same direction in the pores parallel with the external magnetic field. This evidently leads to a high value of *S*. On the other hand, in the pores not parallel with the external magnetic field, the walls and the field tend to orientate LC molecules to different directions. Obviously, the molecules close to walls are parallel with the surface and the molecules in the middle of the pore are tilted more to the direction of the field. As explained later, xenon atom maps all the parts of a pore during NMR measurement, which effectively reduces the value of *S* experienced by the atom. Consequently, the average director of the molecules in the pore is no longer along the pore axis, but it has turned more to the field direction. Therefore, it can be concluded that the more the orientation of the pore differs from the orientation of external magnetic field, the smaller effective *S* in the pore is and the more the orientation of director deviates from direction of pore axis to field direction. This results in the line shape that is not a perfect powder pattern, but the small chemical shift (or large shielding, assuming negative shielding anisotropy) components are absent, and the shape of the signal is more complicated.

One very important factor influencing the observed line shapes is the diffusion of xenon. For the estimation of diffusion distance during the time scale characteristic of an NMR measurement, one can use a simplified two-site system, in which the first site contains nematic phase oriented parallel with the external magnetic field, whereas the orientation in the second phase is perpendicular to the field. As will be shown later, the chemical shift difference of xenon dissolved in these phases is about 10 ppm (~1400 Hz, in the magnetic field of 11.74 T). To see different signals from these two sites, xenon must remain in one site longer than $\tau = 1/\Delta\nu \sim 0.7$ ms.[20] Typical diffusion coefficient of xenon dissolved in LCs is about 10^{-10} m^2/s. Therefore, the distance traveled by a xenon atom during τ is about $(D\tau)^{1/2} \sim 3000$ Å.

The previous estimation means that to see different signals from the phases with different orientations (i.e., from different pores, if the orientation of the pore determines the orientation of LC), the size of one site should be at least 3000 Å. Because in our system the interaction of xenon with pore walls slows down the diffusion, this is the upper limit for the size. The pore size of all the materials used in this study is smaller than 3000 Å, and therefore it is evident that a xenon atom maps the average orientation of LC in a pore, not a local orientation in some part of the pore. Iannacchione et al.[10] estimated from a transmission electron photograph that Vycor glass can be described as a 3D network of randomly connected pores consisting of segments with relatively uniform radius in which the proportion of the length of the segment to the diameter is about 4. Because the structure of the CPG materials used in this study is very similar to that of the Vycor glass with the exception that local deviations from the cylindrical geometry are smaller, it can be assumed that this is true also for those samples, and therefore it can be estimated that the length of pore segment in CPG containing smallest pores (mean diameter 81 Å) is about 300 Å whereas it is about 12 000 Å in CPG containing largest pores (2917 Å). These values imply that the chemical shift of the signal of one xenon atom observed from the materials containing smallest pores is an average of the shifts characteristic of many different pores (and different orientations), whereas the chemical shift of a xenon atom reflects the orientation in one pore in the case of largest pores. In principle, the diffusion averaging could lead to the observation of isotropic signal from the system in which LC molecules form perfect nematic phase inside the pores, if xenon visits a large amount of different pores during the time scale of NMR measurement. The pore segments should then be very short, and the connections between different pore segments would destroy the nematic order.

Restricted geometry affects also the melting point of confined substance. According to the Gibbs-Thompson equation,[21] the melting point depression ΔT is inversely proportional to the pore radius R_p:

$$\Delta T = T_0 - T = \frac{2\sigma_{sl}T_0}{\Delta H_f \rho_s R_p} \equiv \frac{k_p}{R_p} \tag{5}$$

Here, T_0 and T are the melting points of the bulk and confined substance, respectively, σ_{sl} is the surface energy of the solid−liquid interface, ΔH_f is the specific bulk enthalpy of fusion, and ρ_s is the density of the solid. The constant k_p is characteristic to each substance.

Experimental Section

CPG materials were purchased from CPG Inc. (Lincoln Park, NJ). The nominal pore diameters of the materials are 81, 156, 538, 1032, and 2917 Å, and the materials are later referred to with abbreviation CPG followed by pore diameter in angstroms (e.g., CPG 81). The particle size of all the materials is 125−177 μm and according to the manufacturer about 80% of the pores have a diameter within ±9% of the mean pore diameter. Phase 4 LC was obtained from Merck (Darmstadt, Germany). The manufacturer has advised the nematic range of the LC to be 293−347 K. ^{129}Xe isotope enriched (99.95%) xenon gas was delivered by Chemgas (Boulogne, France).

The preparation of the sample was started by putting porous material into a 10-mm medium or heavy wall NMR tube. The material was dried in a vacuum line at the temperature of ~480 K at least 15 h. After that, the tube was removed from the line and was sealed with a plug and Parafilm. Next, Phase 4 was inserted in another similar tube, and gaseous impurities were removed by several freeze−pump−thaw cycles in the vacuum line. When gas bubbles were no longer seen to build up, the porous material was added to the LC, and the system was mixed well and was degassed in the same way as pure LC. Finally, about 3 atm of xenon gas was added to the sample, and the glass tube was sealed with a flame. For the comparison measurements, a sample containing only Phase 4 and 3 atm of xenon gas was also prepared. Before NMR measurements, temperature durability of the samples was tested in an oven at ~380 K.

All the ^{129}Xe NMR experiments were performed on a Bruker Avance DRX500 spectrometer (resonance frequency 138.3 MHz for ^{129}Xe) equipped with a BVT2000 variable temperature unit. A 10-mm high-resolution BBO-probehead was used for one-dimensional measurements, which were carried out on a temperature range ~185−370 K and were performed mainly from low to high temperatures to avoid the supercooling effects of the LC. First, the probehead was cooled with the help of boiling liquid nitrogen to the lowest temperature. Then a sample, which was precooled by immersing it in liquid nitrogen outside the magnet for a couple of minutes, was put into the spectrometer magnet, and it was allowed to stabilize to the set temperature for about an hour. The spectra were recorded applying 30° pulse (the length of the pulse was 8.3 μs), 4.0-s repetition time, −6 dB attenuation, and accumulating 256 scans. The steps of temperature series were 1−5 K and the temperature stabilization time after each step was 20 min. During the measurement, the temperature did not fluctuate more than ±0.1 K. The highest

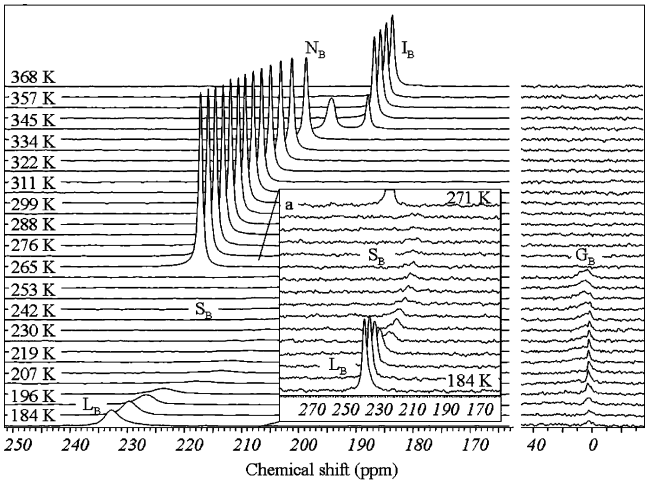

Figure 1. ^{129}Xe NMR spectra measured from the sample containing Phase 4 LC and xenon gas. The measurement temperatures are shown between the spectra. The measurements were done from high to low temperatures. Note that smaller signals in the spectra around 0 ppm and in inset a are represented in different scale.

and the lowest temperatures were calibrated with the aid of ^{1}H NMR spectra from standard temperature calibration samples (4% methanol in deuterated methanol and 80% ethylene glycol in DMSO-D_6) using appropriate correlations between temperature and the chemical shifts of signals.[22] Between these points, the correct temperature was assumed to change linearly as a function of the temperature shown by the VT unit of the spectrometer.

The zero point of the chemical shift scale was set to correspond to the chemical shift of a signal observed from bulk xenon gas sample in which the xenon pressure was 6.16 atm. Signals from the gas sample were measured at the room temperature and at the highest temperature, and the temperature dependency of the resonance frequency of xenon gas was assumed to be linear between these two points.

Small distortions in the baseline of the spectra were manually corrected using the 1D WINNMR program of Bruker.

Assignment of the Signals

Xenon Dissolved in Bulk LC. ^{129}Xe NMR spectra measured at variable temperatures from the sample containing bulk LC and xenon gas are presented in Figure 1. The temperature range is 368−184 K, and these measurements were exceptionally done from high to low temperatures. The different signals have been labeled in the figure. In all the spectra presented, the label of signals contains a capital letter (or many letters), which refers to the phase sampled by a xenon atom (I = isotropic, N = nematic, S = solid, G = gas, and L = liquefied), and a subscript, which refers to whether the signal arises from inside the pore (subscript C, an abbreviation for confined) or from outside the porous material (subscript B, an abbreviation for bulk). In addition, when many solid phases are observed from the sample, they are numbered, and the number follows the capital letter in the label (for example, $S1_B$). The origins of the signals in Figure 1 will be analyzed below.

Signal I_B. A sharp, Lorentzian signal is observed from the isotropic phase of Phase 4 LC. Chemical shift of signal I_B increases linearly from 183.6 to 187.9 ppm when temperature decreases from 368 to 345 K.

Signal N_B. At 345 K, a signal (denoted by N_B) from xenon dissolved in the nematic phase of the LC appears in the spectrum at ∼6.4 ppm larger chemical shift than signal I_B. Both nematic and isotropic regions exist in the sample at that temperature. This is a commonly observed phenomenon near isotropic−nematic phase-transition point of LCs and is mainly a result of a small temperature gradient over the sample. The phase-transition temperature is very close to the temperature announced by the manufacturer (347 K). The chemical shift of signal N_B increases from 194.3 to 217.1 ppm as temperature decreases from the transition point to 271 K because of increase of orientational order and density of LC in nematic phase. The signal disappears when the LC freezes. According to the spectra, the freezing point is about 270 K. Because the melting point of Phase 4 announced by the manufacturer is 293 K, it can be concluded that the nematic−solid phase-transition temperature has shifted over 20 K to lower temperature because of supercooling of the LC.

Signal S_B. During nematic−solid transition, a majority of xenon atoms squeeze out from the solid and only a very small signal (denoted by S_B) is observed from xenon atoms occluded by solid LC.

Signal G_B. Below the freezing point of the LC, a small signal (denoted by G_B) appears close to the chemical shift of bulk xenon gas (0 ppm). This implies that the signal originates from xenon gas in relatively large voids built up during the freezing transition. Evidently, the LC contracts somewhat during the transition because of the slight increase in its density, and an empty layer builds up between the solid LC and the wall of the sample tube. At least a part of the signal G_B arises from xenon in that layer. The rest of the signal may arise from large bubbles formed inside the solid. The fast pulsing rate used in the measurements may lead to a partial saturation of the signal, because the spin−lattice relaxation time, T_1, of gaseous xenon is very long; it may be even 3 h for bulk gas.[23] This may decrease the intensity of signal G_B.

Signal L_B. Below 202 K, a broad signal (signal L_B, fwhm ∼ 5 ppm) appears around ∼224 ppm. From the chemical shift value, it can be deduced that the signal originates from the liquefied xenon. According to the xenon vapor pressure diagram, bulk xenon gas liquefies at 186 K at the pressure of 3 atm.[24] Inside the small volumes, the condensation may appear at higher temperatures.

Another temperature series were measured from the same sample from low to high temperatures in the same way as described in the Experimental Section. The spectra are shown in Figure 2. The different temperature history, especially immersing the sample in liquid nitrogen before the measurement, causes drastic changes on the signals observed from solid phase. The origins of the signals are discussed below.

Generally, the integrated intensities of the signals observed below the melting point of the LC in Figure 2 are many times larger than those of the corresponding signals in Figure 1, and they are quite close to the value of that in the nematic phase. This implies that, during the abrupt freezing of the LC outside of the magnet, xenon atoms do not squeeze out from the LC to as large extent as during the gradual freezing. Instead, most of the atoms are occluded inside the solid matrix of the LC.

Signal $S1_B$. At the lowest temperatures in Figure 2, a signal in the chemical shift region of liquefied xenon is seen. On the other hand, its behavior differs substantially from that of signal L_B in Figure 1. First, the fwhm of the signal is very large. It is about 68 ppm at 184 K and about 38 ppm at 202 K whereas it is about 3 ppm in Figure 1 within the whole temperature range of the signal. Second, the chemical shift of the signal stays almost constant (∼217 ppm), whereas it increases about 9 ppm in Figure 1 when the temperature decreases from 202 to 184 K. Third, the intensity of signal L_B increases gradually with

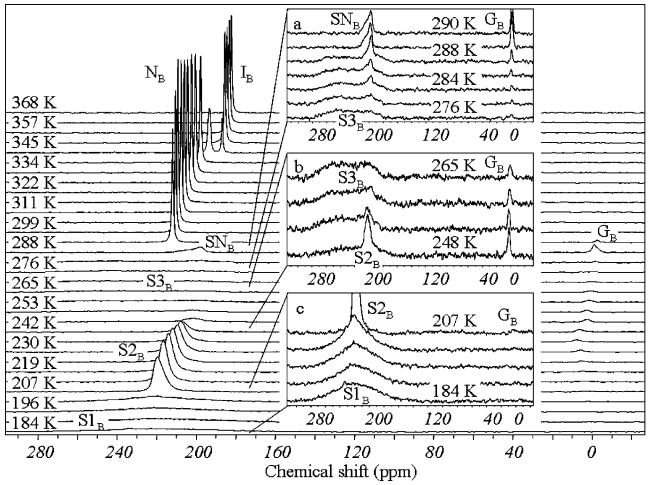

Figure 2. ^{129}Xe NMR spectra measured from the same sample and temperature region as in Figure 1, but in this case, the sample was first frozen outside the magnet by liquid nitrogen and the measurements were done from low to high temperatures. Note the different scale in the insets.

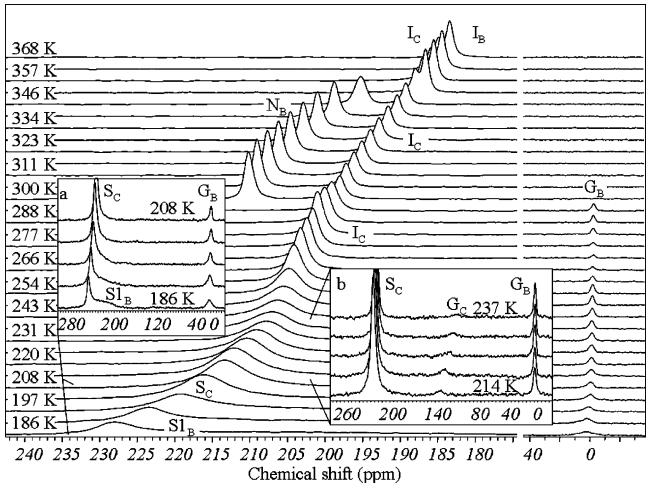

Figure 3. ^{129}Xe NMR spectra measured from the sample containing CPG 81, Phase 4, and xenon gas. Note the different scales in the insets.

decreasing temperature in Figure 1 because the gas−liquid transition of xenon takes place gradually, whereas no gradual decrease of the intensity with increasing temperature is observed in Figure 2. Instead, an abrupt growth of the signal is observed at 207 K, which is not typical of liquid−gas transition of xenon. Therefore, it can be concluded that the signal does not originate from the conventional liquid phase of xenon. Instead, the behavior of the signal implies that it arises from the atoms occluded inside the solid matrix. Hence, the signal has been labeled as $S1_B$ in Figure 2. The large line width of the signal may reflect the short spin−spin relaxation time, T_2, of occluded xenon, the size distribution of the sites where xenon atoms are occluded, or the crystal structure of the solid in the surrounding of xenon atoms.

Signal $S2_B$. At 207 K, the wide signal $S1_B$ converts into the relatively sharp, Lorentzian signal denoted by $S2_B$. Because it was deduced above that this substantial and abrupt change cannot be a consequence of liquid−gas transition of xenon, the only realistic explanation is that the solid−solid phase transition takes place in the LC surrounding the xenon atoms. Unfortunately, we did not find any information about the solid phases of Phase 4 LC from literature. However, the Lorentzian line shape of the signal implies that the crystal structure of the new solid phase above 207 K is more symmetrical than that of the previous one. The signal exists in the temperature range 207−253 K, its chemical shift decreases from 217 to 201 ppm in that range, and the line width stays nearly constant (about 6 ppm).

Signal $S3_B$. Near 250 K, signal $S2_B$ disappears and a new, very broad signal (denoted by $S3_B$) grows up around 240 ppm. The line width of the signal is about 80 ppm. This drastic change in the signal shape implies that the second solid−solid phase transition takes place in the LC surrounding the xenon atoms and the new crystal structure is substantially more asymmetric than the previous one. The signal exists from 248 to 287 K, and its chemical shift and line width stay nearly constant.

Signal SN_B. A few degrees below the solid−nematic phase transition, signal $S3_B$ disappears and signal SN_B grows up. The shape of signal SN_B is asymmetric. Evidently, signal SN_B relates to pretransitional effects of the solid−nematic transition. Small nematic droplets build up inside the solid. In the restricted space, the interactions of LC molecules with solid LC phase define the direction of the director of the nematic phase instead of the external magnetic field. Because the orientation of the director is different in the different droplets and because the distribution of the orientations is isotropic, axially symmetric anisotropic CSA powder spectrum (i.e., signal SN_B) is observed.

Signals N_B and I_B observed above the solid−nematic and nematic−isotropic phase transitions behave in the same way as in Figure 1. Signal G_B arises from gaseous xenon as in the case of Figure 1. The intensity of signal G_B increases considerably when signal SN_B appears. This indicates that when small nematic droplets build up, a part of xenon atoms occluded in the solid phase is released to relatively large bubbles, increasing the intensity of signal G_B. The bubbles (and signal G_B) disappear when the solid LC melts. On the basis of the disappearance of signal G_B and the build-up of signal N_B, it can be concluded that the solid−nematic phase transition takes place at 291 K, which is close to the temperature announced by the manufacturer (293 K). Phase-transition temperatures from nematic to isotropic as well as the chemical shift difference of signals N_B and I_B are equal in Figures 1 and 2.

LC in Small Pores (about Molecular Size). ^{129}Xe NMR spectra measured from the sample containing CPG 81, Phase 4, and xenon gas are shown in Figure 3. The spectra (as well as all the rest of the spectra shown below) were measured from low to high temperatures in the way explained in the Experimental Section. Since the structural characteristics of the CPG matrix are nearly temperature-independent in the measurement range, all the observed temperature-dependent effects can be attributed to the change in the physical properties of the LC.

The signals observed below bulk melting point will be analyzed first. Generally, the different regions are not seen in this figure as clearly as in the case of bulk LC in Figure 2. One big signal around 200−230 ppm dominates the spectrum, and evidently it arises from pores, because its behavior cannot be associated with the signals observed from bulk LC in Figure 2. However, a closer inspection shows that the same signals as in Figure 2 exist in the spectra. This can be expected, because LC between the particles of porous material behaves like bulk LC. Signal $S1_B$ is seen at the lowest temperatures around 207 ppm (see inset a). In Figure 2, signal $S2_B$ appears at the temperature range of ∼207−253 K, and its chemical shift decreases from 217 to 201 ppm in that interval. In this figure, the signal seems to coincide with the large signal from the pores. Signal G_B originating from relatively large bubbles or pockets built up between the particles of porous materials because of the

contraction of LC in liquid−solid transition is also seen in the spectra below the bulk melting point.

At the lowest temperatures, the signal arising from xenon occluded in solid LC inside the pores is denoted by S_C. The fact that there are no discontinuities in the chemical shift or intensity behavior of signal S_C as a function of temperature implies that no first-order solid−solid phase transitions take place inside the pores. According to the Gibbs-Thompson equation (eq 5), the melting point of a substance confined to a small pore is lower than that of a bulk substance. Therefore, the increase in the amplitude of the signal from the pores at around 260 K can be associated to melting of confined LC. The melting point depression is about 38 K. Because the signal observed above that temperature is Lorentzian and relatively narrow, the phase of LC surrounding xenon atoms seems to be isotropic or xenon senses on average an isotropic environment inside the pores, and therefore the signal has been denoted by I_C. A tiny signal G_C is observed below the melting point of confined LC (see inset b in Figure 3). From its chemical shift, it can be deduced that the signal arises from the gas inside very small voids. Evidently, the signal arises from tiny pockets built up inside the pores because of the contraction of LC in freezing transition. This kind of pockets has also been observed when porous materials have been immersed in isotropic liquids.[25−27] The signal is weak, because only a very small part of xenon atoms release from solidifying liquid to the pockets during rapid freezing of the sample. In addition, the large chemical shift of the signal indicates that the pockets are very small, which may be a consequence of a relatively small change of density of LC during freezing, and this makes the intensity of the signal even smaller. Signal G_C is not observed from every sample. The reason for this may be that the freezing of some samples was more rapid, and therefore xenon atoms did not squeeze out from the solidifying LC at all.

During the melting of bulk LC, the signal of xenon occluded in the solid disappears. Furthermore, signal G_B disappears, because the pockets between the particles of porous materials are filled by liquid. Signal I_C is still observed from the liquid inside the pores. Signal N_B, arising from the nematic phase between the particles, grows up and its chemical shift is ∼10 ppm larger than that of I_C. The fact that its chemical shift and line shape behavior as a function of temperature are similar to those in bulk LC cases in Figures 1 and 2 confirms that the LC between the particles behaves like bulk LC.

During the nematic−isotropic phase transition (∼347 K), signal N_B disappears and signal I_B grows up at ∼6.7 ppm smaller chemical shift value. Its chemical shift is exactly the same as in the case of bulk liquid. Chemical shift of signal I_C is about 1.5 ppm larger than that of signal I_B. The larger shift of signal I_C is a consequence of direct or indirect interactions of xenon atoms with the surface of the pores.

LC in Large Pores (about Magnetic Coherence Length). ^{129}Xe NMR spectra measured from the sample containing CPG 2917, Phase 4, and xenon gas are shown in Figure 4. Below the bulk melting point, the spectra resemble very much those measured from bulk LC (see Figure 2). There is an $S1_B$-like signal at the lowest temperatures, and an $S2_B$-like signal appears in the spectra in the temperature range of 208−247 K. Above that range, a wide, $S3_B$-like signal builds up and is seen until the melting point of bulk LC. Because those signals dominate the spectra and because there is no other signal that could be associated to arise from the pores, it can be concluded that the LC inside the pores behaves like bulk LC, that is, the solid phases have similar structure as in bulk, and the solid−solid

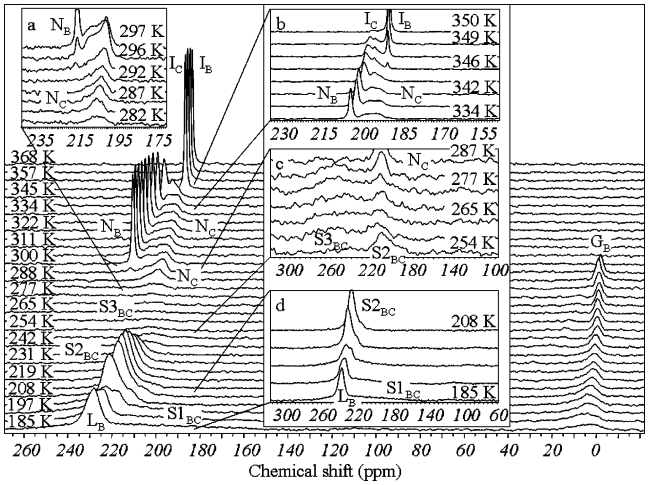

Figure 4. ^{129}Xe NMR spectra measured from the sample containing CPG 2917, Phase 4, and xenon gas. Note the different scales in the insets.

phase transitions take place at the same temperatures. Therefore, all those signals have been labeled in these spectra by SX_{BC}, where X is the number of solid phase (1, 2, or 3). The subscript BC has been used because it cannot be distinguished whether the signal arises from pores or from outside the porous materials. However, there are also two remarkable differences between the spectra in Figures 2 and 4: the intensity of signal G_B is much larger in Figure 4 and at the lowest temperatures there is an additional signal around 230 ppm. The only conceivable explanation for the large intensity of signal G_B is that there must be exceptionally many gas bubbles in the sample for some unknown reason. Actually, the signal around 230 ppm may be also a consequence of the bubbles, because it might arise from the liquefied xenon inside the bubbles. Therefore, the signal has been labeled by L_B. Bulklike solid phases seem to appear also in CPG 538 and 1032 samples. However, the intensity of signal G_B is much smaller in those samples, and signal L_B does not appear at all, which supports the previous interpretation. At ∼282 K, an asymmetric signal begins to gradually grow up at around 200 ppm. Evidently, the build-up of the signal is a consequence of solid−nematic phase transition of LC inside the pore, and therefore the signal is denoted by N_C. The direction of the director of nematic phase inside the pore is mainly determined by the interaction of the LC molecules with the surface of pores, and because of isotropic orientation distribution of the pores in the samples, CSA powder pattern line shape is observed.

Above the bulk melting point, signal N_C becomes gradually narrower and finally, at the highest temperatures of nematic range, it loses its powder pattern line shape. The elastic constant K decreases rapidly with increasing temperature.[28] According to eq 2, magnetic coherence length ξ_M is directly proportional to K. Hence, ξ_M decreases with increasing temperature. The pore size of CPG 2917 is on the same order of magnitude with ξ_M. Therefore, the changes in the shape of the signal can be associated with the temperature dependence of ξ_M. As ξ_M becomes smaller with increasing temperature, the average orientation of LC inside a pore deviates more from the direction of pore axis to the direction of external magnetic field. The small chemical shift components of signal N_C disappear, and this destroys gradually the powder shape of the signal, as described earlier. This kind of behavior is clearly seen in Figure 4, and at the highest temperatures of nematic phase, signal N_C almost merges together with signal N_B (see inset b in Figure

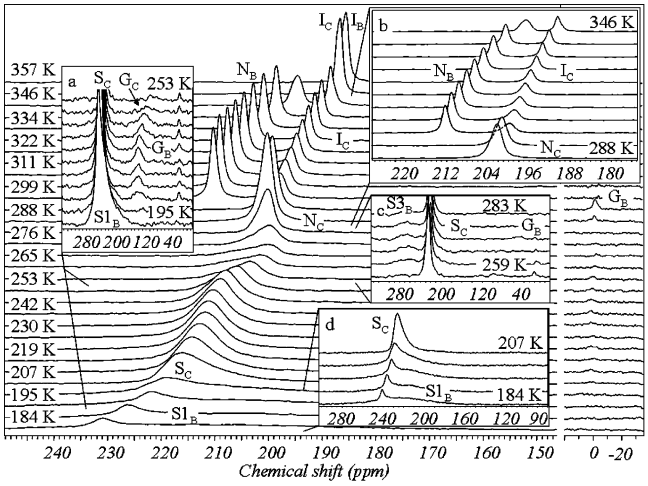

Figure 5. The ^{129}Xe NMR spectra measured from the sample containing CPG 156, Phase 4, and xenon gas. Note the different scales in the insets.

4), which indicates that the director inside the pores is almost parallel with the external magnetic field. Above the nematic−isotropic phase transition, only one signal is seen in the spectra. The interactions of xenon with the pore walls are weak because of large pore size, and therefore signals I_C and I_B coalesce.

LC in the Medium-Size Pores. ^{129}Xe NMR spectra measured from the sample containing CPG 156, Phase 4, and xenon gas are shown in Figure 5. All the same signals are seen in the spectra as in the case of CPG 81 (see Figure 3). Signal S_C from xenon occluded in solid LC inside the pores is seen until higher temperatures than in the case of CPG 81 because the melting point depression of confined LC is smaller in CPG 156. There are not as clear evidences for solid−solid phase transitions inside the pores as in the case of CPG 2917, but nonlinear temperature behavior of signal S_C around 250 K might be a consequence of gradual, higher order transition. Confined LC begins to melt at around 280 K, as can be deduced from the change of intensity of the signal arising from the pores. The shape of the signal arising from melted LC inside the pores is first slightly axially symmetric CSA powder pattern, but it gradually becomes Lorentzian with increasing temperature. This may mean that because of increased diffusion averaging as a consequence of increased diffusion coefficient of xenon with increasing temperature, xenon visits a larger number of differently oriented pores during the time scale of NMR measurement as temperature is increased and consequently senses isotropic environment on average. The second, more probable option is that the size of the pores in CPG 156 is just large enough for building up a nematic phase, when temperature is low enough, but the phase changes gradually to isotropic when temperature is raised. The signal is therefore denoted by I_C at higher temperatures and N_C at lower temperatures. Above bulk nematic−isotropic transition, signals I_B and I_C almost merge together, because the interactions of confined xenon atoms with the pore walls are weak in relatively large pores.

Analysis

Temperature Dependence of ^{129}Xe NMR Shielding in the Bulk LC. Equation 4 represents how the shielding of dissolved xenon behaves as a function of temperature. Before the use of eq 4, the zero point of shielding (or chemical shift) scale was extrapolated to the chemical shift of xenon gas at zero pressure. This was done with the following equation:[29]

$$\sigma(\rho, T) = \sigma_0 + \sigma_1(T)\rho + \sigma_2(T)\rho^2 + \sigma_3(T)\rho^3 \qquad (6)$$

In eq 6, σ_0 is the shielding in a vacuum and ρ is the density in amagat units. The temperature-dependent virial coefficients σ_1, σ_2, and σ_3 represent two, three, and four body interactions, respectively. At low densities (pressures), however, only the first virial coefficient is relevant.[29]

Because eq 4 represents purely the microscopic part of the effects of solvent on the shielding of solute, the macroscopic bulk susceptibility correction σ_b has to be taken into account. The susceptibility effect in a long cylindrical sample parallel with the applied magnetic field is[30]

$$\sigma_b = -\frac{1}{3}\left[\chi + \frac{2}{3}\Delta\chi S(T)\right]\frac{\rho(T)}{M} \qquad (7)$$

where χ and $\Delta\chi$ are the isotropic part and anisotropy of the diamagnetic susceptibility tensor, respectively, and M is the molar mass of LC.

The use of eq 4 requires knowledge about the density behavior of LC. Unfortunately, this information is not available for Phase 4 LC. However, a good approximation is that the density changes linearly as a function of temperature both in isotropic and nematic phases.[31] In isotropic phase, the density behavior can be approximated by the function $\rho(T) = \rho_0[1 - \alpha(T - T_0)]$, where ρ_0 is the density at the reference temperature T_0, and α is the isobaric thermal expansion coefficient. In the nematic phase, the density can be modeled by equation $\rho(T) = \rho_0\{[1 - \alpha(T - T_0)] + \Delta\rho/\rho_0\}$, where $\Delta\rho$ represents the density jump in the isotropic−nematic phase transition. Coefficient α may be different in the isotropic and nematic phases.

Because the angle between the LC director **n** and the external magnetic field $\mathbf{B}_0$ is zero in bulk nematic phase, the value of function $P_2(\cos\theta)$ in eq 4 is 1. The temperature dependence of the second-rank orientational order parameter in nematic phase can be modeled by the Haller function $S(T) = (1 - yT/T_0)^z$, where y and z are adjustable parameters.[32]

By inserting the density functions, Haller function, and eq 7 in eq 4, the average of the shielding tensor element in isotropic phase reduces to

$$\langle\sigma_{ZZ}\rangle_{iso} = \rho_0[1 - \alpha(T - T_0)]\left\{\sigma_0[1 - \beta_1(T - T_0)] - \frac{\chi}{3M}\right\} \qquad (8)$$

In anisotropic phase, eq 4 becomes

$$\langle\sigma_{ZZ}\rangle_{aniso} = \rho_0\left\{[1 - \alpha(T - T_0)] + \frac{\Delta\rho}{\rho_0}\right\} \times \left\{\sigma_0[1 - \beta_1(T - T_0)] + \frac{2}{3}\Delta\sigma_0[1 - \beta_2(T - T_0)] \times \left(1 - y\frac{T}{T_0}\right)^z - \frac{1}{3M}\left[\chi + \frac{2}{3}\Delta\chi\left(1 - y\frac{T}{T_0}\right)^z\right]\right\} \qquad (9)$$

In the least-squares fits of eqs 8 and 9 to measured shielding data (measured from the low to high temperature), the nematic−isotropic phase transition temperature T_{NI} was used as reference temperature T_0 ($T_0 = T_{NI} = 345.2$ K). The used values for χ and $\Delta\chi$ were $-2.40\cdot10^{-9}$ m^3/mol and $0.43\cdot10^{-9}$ m^3/mol, respectively, which are typical for molecules with two benzene rings.[31] Molar mass of Phase 4 is 284.15 g/mol. First, parameters ρ_0, α, σ_0, and β_1 were resolved by fitting eq 8 to the shielding data obtained from the isotropic phase. Then, eq 9 was fitted to the shielding data of the nematic phase. In this fitting, parameters ρ_0, σ_0, and β_1 were kept fixed to the values obtained from the

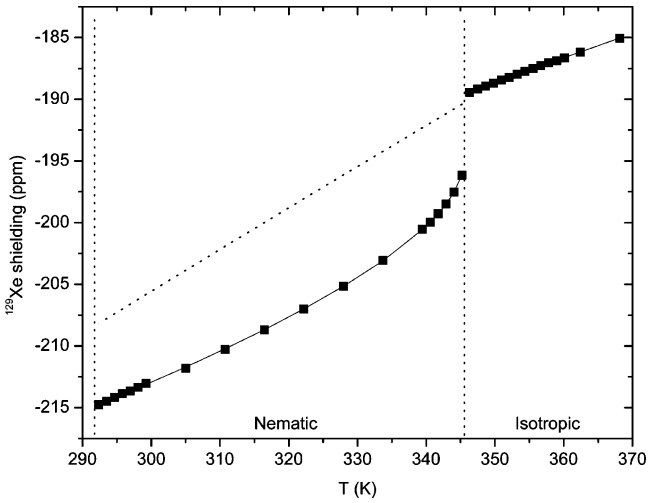

Figure 6. Shielding of ^{129}Xe in the bulk LC Phase 4 referenced to zero pressure xenon gas as a function of temperature (■). The solid lines represents the least-squares fits of eq 8 and 9 in the isotropic and nematic phases, respectively. The calculated isotropic average of the shielding tensor in the nematic phase, i.e., the first part of eq 9 is depicted by dotted line. Vertical dash lines indicate phase-transition temperatures.

TABLE 1: Values of the Parameters Obtained by Fitting of Eqs 8 and 9 to the Experimental ^{129}Xe Shielding Data for Xenon in Bulk Phase 4 Liquid Crystal

parameter	isotropic phase	nematic phase
$T_0 = T_{NI}/K$	345.2[a]	345.2[a]
ρ_0/g cm^{-3}	0.964	0.964[b]
$\Delta\rho_0/\rho$ (%)		0.42
$\alpha/10^{-4}$ K^{-1}	5.39	12.16
σ_0/ppm cm^3 g^{-1}	−199.537	−199.537[b]
$\beta_1/10^{-4}$ K^{-1}	5.14	5.14[b]
$\beta_2/10^{-4}$ K^{-1}		−104.71
$\Delta\sigma_0$/ppm cm^3 g^{-1}		−30.35
y		0.998
z		0.209

[a] Fixed (see the text). [b] Fixed to the value obtained from isotropic phase.

isotropic phase, and parameters α, $\Delta\rho$, $\Delta\sigma_0$, β_2, y, and z were kept as free variables. The measured shielding data together with fitting curves are shown in Figure 6. The values of the adjusted parameters are collected in Table 1.

Almost equal values of α ($5.39\cdot10^{-4}$ K^{-1}) and β_1 ($5.14\cdot10^{-4}$ K^{-1}) in the isotropic phase indicate that the change of solvent density and Xe−Phase 4 molecule pair correlation function have equal contribution to the temperature dependence of the ^{129}Xe shielding. On the contrary, the value of α ($12.16\cdot10^{-4}$ K^{-1}) obtained in the nematic phase is significantly larger than β_1, which implies that the temperature dependence of the isotropic part of xenon shielding in eq 9 depends more on the change of solvent density. The opposite sign and much larger value of β_2 ($-104.71\cdot10^{-4}$ K^{-1}) as compared with α ($12.16\cdot10^{-4}$ K^{-1}) reveal that the solute−solvent pair correlation has a dominant role in the change of the anisotropic part of the shielding. This means that the average anisotropy of the local shielding tensor decreases as a function of decreasing temperature and consequently anisotropic part of the shielding has opposite temperature dependence to that of the isotropic part. The isobaric thermal expansion coefficients are consistent with those observed from other thermotropic nematogens.[31,33,34]

Chemical Shift of ^{129}Xe and Orientation Order of LC inside the Pores. The chemical shifts of xenon resonance signals observed from different samples in the temperature range 285−370 K are shown in Figure 7. In the case of powder pattern line shape spectra, the isotropic chemical shifts value δ_{iso} has been used in the figure. As shown above, first-order isotropic−nematic phase transition is accompanied by an abrupt change in the density of the LC. Apart from this phenomenon, also the anisotropy of the diamagnetic susceptibility tensor and the anisotropy of the ^{129}Xe shielding tensor are switched on at the phase transition. These three factors together cause the discontinuity in the chemical shift versus temperature curve. The anisotropy of the shielding tensor arises from the fact that the anisotropic force acting in mesophases deforms the originally spherical electron distribution of xenon.

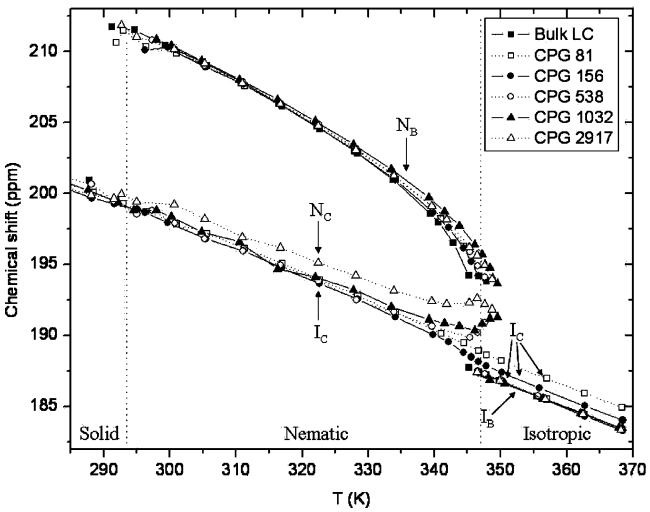

Figure 7. Chemical shift of xenon dissolved in Phase 4 confined to five different CPG materials as a function of temperature. The data points from bulk LC sample are also shown in the figure. The lines between the symbols are to guide the eye. Vertical dash lines indicate phase-transition temperatures of bulk LC announced by the manufacturer. All the measurements were done from low to high temperature.

The chemical shift of signal originating from CPG 81 changes very linearly as a function of temperature in the whole temperature region, which supports the earlier interpretation that the phase inside the pores remains isotropic-like below bulk isotropic−nematic transition. Actually, the isotropic line shape is not a definite evidence of isotropic phase inside the pores, because in principle $P_2(\cos\theta)$ term in eq 4 might average zero because of fast exchange of xenon between different pores, as explained earlier. However, the linear temperature dependence of the chemical shift of the signal signifies unambiguously that no isotropic−nematic phase transition takes place inside CPG 81 material. Similar results have also been observed in other studies of LCs confined to sufficiently restrictive pores.[14,19,35]

Chemical shift versus temperature behavior of the signal arising from CPG 156 is not completely linear below bulk isotropic−nematic transition point. The curvature of the chemical shift curve supports the earlier interpretation on the basis of the gradual increase of anisotropy of line shape that the nematic phase builds up gradually inside the pore with decreasing temperature.

There is a clear discontinuity point in the chemical shift behavior of the signals observed from CPG 538, 1032, and 2917. This means that a bulklike first-order isotropic−nematic phase transition takes place inside those relatively large pores. The transition temperature is close to that of bulk transition. The average chemical shift of the signal arising from CPG 2917 is larger than that observed from the other samples. This supports also the conclusions drawn on the basis of line shape, that is, the pore size in CPG 2917 is close to magnetic coherence length

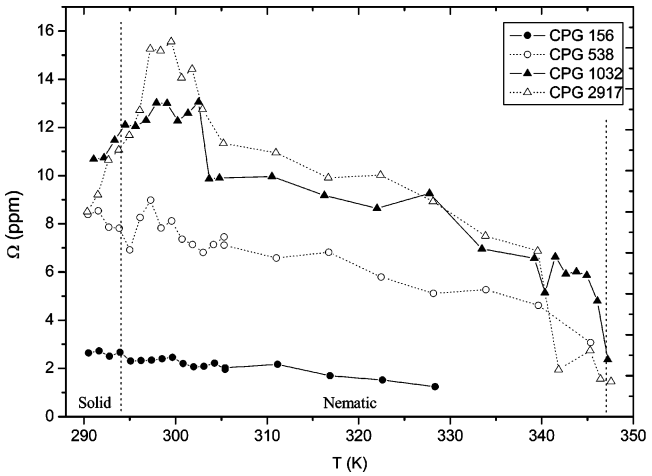

Figure 8. Span of the ^{129}Xe powder patterns observed from the pores of different size as a function of temperature. The lines between the symbols are to guide the eye. Vertical dash lines show phase-transition temperatures of bulk LC.

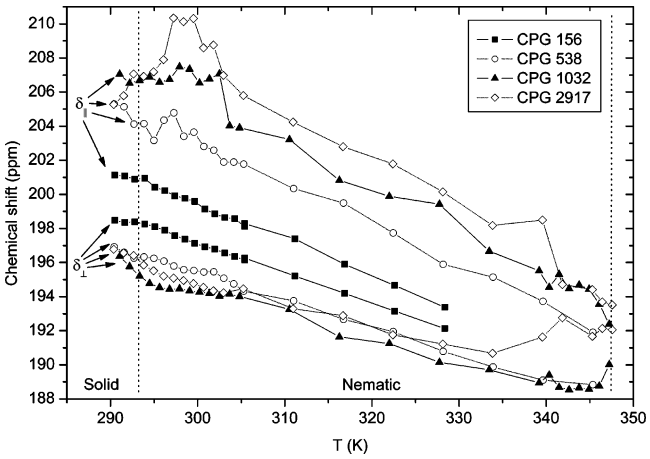

Figure 9. Parallel ($\delta_{||}$) and perpendicular ($\delta_{\perp}$) ^{129}Xe chemical shift components as a function of temperature measured from the samples containing different porous materials. The lines between the symbols are to guide the eye. Bulk-phase-transition temperatures are denoted by vertical dash lines.

ξ_M, and therefore the orientation of the LC molecules deviates from pore axis direction to magnetic field direction, and this increases the average chemical shift of the signal. Because ξ_M decreases with increasing temperature, the chemical shift of the signal approaches that of the signal observed from bulk nematic, in which case the director is parallel with the external magnetic field. The chemical shifts of the signals originating from CPG 1032 and 538 curve also slightly upward when approaching the nematic−isotropic transition, indicating that also inside these materials magnetic field changes slightly the orientation of director of nematic phase.

Because the particles of porous materials are relatively large, the chemical shifts of signals observed outside the materials are close to those observed from bulk LC. Small deviations seen in Figure 7 may be mainly due to inaccuracy in temperature determination in the measurements (~2 K).

Parallel and perpendicular chemical shift components of the ^{129}Xe powder pattern spectra are defined as $\delta_{||} = \delta_{iso} + {}^2/_3\Delta\delta$ and $\delta_{\perp} = \delta_{iso} - {}^1/_3\Delta\delta$, respectively. The span, $\Omega = \Delta\delta = \delta_{||} - \delta_{\perp}$ (the span and chemical shift anisotropy are equal for an axially symmetric powder pattern), of the signals observed from the pores has been plotted as a function of temperature in Figure 8. On the basis of the figure, it can generally be concluded that the larger the pore size is the larger the span is. This kind of behavior may mainly be a consequence of the increase of value of order parameter *S* with increasing pore size, because small pore size and small distance between intersections of different pores disturb the orientation of the LC molecules. In addition, the diffusion averaging is most remarkable in the materials containing the smallest pores because of short distance between the pores. This effectively decreases the *S* value experienced by a xenon atom. The span of the signal arising from CPG 2917 decreases much at higher temperatures, because LC molecules orientate on average more to the direction of external magnetic field in the pores. This leads to the powder pattern line shape that deviates from the axially symmetric one. In addition, parameter *S* experienced by a xenon atom may decrease slightly because LC molecules near the surface of pores are parallel with the surface, but in the middle of the pore the molecules align more to the magnetic field direction, and this decreases span as well.

Parallel and perpendicular chemical shift components of the powder pattern spectra in different CPG samples as a function of temperature have been plotted in Figure 9. $\delta_{||}$ and $\delta_{\perp}$ increase almost linearly with decreasing temperature mainly because of the increase of density of LC. At a certain temperature, parallel component $\delta_{||}$ increases with increasing pore size, which reflects the increase of (effective) order parameter *S*, as discussed earlier. The decrease of perpendicular component $\delta_{\perp}$ with increasing pore size in the case of smaller pores is a consequence of the same phenomenon. However, $\delta_{\perp}$ of CPG 2917 is larger than that of CPG 1032 (or even that of CPG 538 at higher temperatures). This is again a consequence of change of the average LC orientation to the direction of external magnetic field in the largest pores, which especially reflects to $\delta_{\perp}$ component. The decrease of magnetic coherence length with increasing temperature can be clearly seen in the $\delta_{\perp}$ behavior of CPG 2917 at higher temperatures.

Effects of Confinement on Solid-Phase Transitions. Below the nematic−solid phase transition, two solid−solid transitions in bulk LC can be detected (see Figure 2). The transition temperature of LC inside the pores is lower than that of bulk LC. The phase-transition temperatures were found to extend over a wide temperature range because of distribution of pore sizes in the samples. In larger pores, phase transition takes place at a higher temperature than in smaller pores, resulting in a temperature distribution. From the changes in the intensity or amplitude of the signal arising from the pore, it can be deduced that the melting point depressions, ΔT, in CPG 81, 156, and 538 are about 38, 15, and 5 K, respectively. ΔT was not determined from CPG 1032 and 2917 because it is so small that the changes in the signals can be disturbed by the pretransitional effects discussed earlier. Least-squares fit of Gibbs-Thompson equation (eq 5) to these data points results in the k_p value of 1345 KÅ. This is a very large value as compared with the values determined from conventional liquids (for example, for acetonitrile and cyclohexane k_p is 545 and 724 KÅ,[36,37] respectively). The sensitivity of the melting point depression to pore size can be used for pore size determination of unknown materials, as is done, for example, in NMR cryoporometry.[38]

The same solid phases as observed in bulk LC are also observed in CPG 538−2917 samples, and the solid−solid phase-transition temperatures are the same. However, the xenon signal observed from the pores implies that no first-order solid−solid phase transitions takes place in CPG 81 and 156 samples. Instead, even nematic−solid transition seems to be a gradual, higher order phase transition. The nonlinear behavior of the

chemical shift of the signal as a function of temperature observed from CPG 156 around 250 K may be a consequence of another higher order phase transition. On the basis of previous discussion, it can be concluded that the size of pore must be at least ~500 Å in order that bulklike solid LC phase could be formed inside the pore.

Conclusion

In this study, we have shown that ^{129}Xe NMR of xenon gas dissolved in LCs can give versatile information about the orientation distribution of LCs confined to the pores. According to the results, the size of the pores must be approximately 10 times larger than molecular length to observe nematic−isotropic phase transition inside the pores. Above that size (~150 Å), nematic phase is seen inside the pores and the effective orientation parameter *S* experienced by xenon atoms increases with increasing pore size. In case of the largest pores, the spectra show that the LC molecules are oriented more to the direction of the external magnetic field inside the pores, which implies that the pore size (2917 Å) is close to magnetic coherence length. The decrease of the magnetic coherence length with increasing temperature is clearly seen from the spectral parameters. A model based on pairwise additivity approximation developed by Ylihautala et al.[16] has been shown to explain the temperature dependence of the shielding of ^{129}Xe dissolved in bulk Phase 4, and it has also been very useful in explaining the behavior of LC inside the pores.

This study shows also that when the sample is cooled very rapidly by immersing it in liquid nitrogen, xenon atoms do not squeeze out from the solid but the atoms are occluded by the solid. The resonance signal of those atoms reflects clearly the structure of the solid. This makes also possible to determine how the confinement affects the two solid−solid phase transitions observed in bulk LC in the measurement temperature range. According to the spectra, the solid phases inside the pores are similar to those in bulk LC, when the pore size is above ~500 Å. In the smaller pores, no first-order solid−solid phase transitions are observed. The melting point depression (i.e., the depression of solid−nematic phase transition of LC inside the pores as compared with that in bulk LC) has been found to be extraordinary sensitive to pore size, and this sensitivity can be used for determining the pore size of unknown material.

Acknowledgment. The authors are grateful to the Academy of Finland (grants 43979 and 203278) and the Graduate School of Computational Chemistry and Molecular Spectroscopy (LASKEMO) for financial support. P.T. acknowledges the grants from the Research Foundation of Orion Corporation, Tauno Tönning Foundation, and Oskar Öflunf Stiftelse. V.-V.T. appreciates Helsingin Sanomain 100-Vuotissäätiö for financial support.

References and Notes

(1) Crawford, G. P.; Žumer, S. *Liquid Crystals in Complex Geometries Formed by Polymer and Porous Networks*; Taylor and Francis: London, 1996.

(2) Bellini, T.; Clark, N. A.; Muzny, C. D.; Wu, L.; Garland, C. W.; Schaefer, D. W.; Oliver, B. J. *Phys. Rev. Lett.* **1992**, *69* (5), 788.

(3) Guégan, R.; Morineau, D.; Loverdo, C.; Béziel, W.; Guendouz, M. *Phys, Rev. E* **2006**, *73*, 011707.

(4) Shao, Y.; Zerda, T. W. *J. Phys. Chem. B* **1998**, *102*, 3387.

(5) Dadmun, M. D.; Muthukumar, M. *J. Chem. Phys.* **1993**, *98* (6), 4850.

(6) Tripathi, S.; Rosenblatt, C.; Aliev, F. M. *Phys. Rev. Lett.* **1994**, *72* (17), 2725.

(7) Hsiung, H.; Rasing, T.; Shen, Y. R. *Phys. Rev. Lett.* **1986**, *57* (24), 3065.

(8) Zidansek, A.; Lahajnar, G.; Kralj, S. *Appl. Magn. Reson.* **2004**, *27* (1−2), 311.

(9) Long, H. W.; Luzar, M.; Gaede, H. C.; Larsen, R. G.; Kritzenberger, J.; Pines, A.; Crawford, G. P. *J. Phys. Chem.* **1995**, *99*, 11989.

(10) Iannacchione, G. S.; Crawford, G. P.; Žumer, S.; Doane, J. W.; Finotello, D. *Phys. Rev. Lett.* **1993**, *71* (16), 2595.

(11) Golemme, A.; Žumer, S.; Allender, D. W.; Doane, J. W. *Phys. Rev. Lett.* **1988**, *61* (26), 2937.

(12) Crawford, G. P.; Yang, D. K.; Žumer, S.; Finotello, D.; Doane, J. W. *Phys. Rev. Lett.* **1991**, *66* (6), 723.

(13) Jin, T.; Zalar, B.; Lebar, A.; Vilfan, M.; Žumer, S.; Finotello, D. *Eur. Phys. J. E* **2005**, *16*, 159.

(14) Iannacchione, G. S.; Qian, S.; Finotello, D.; Aliev, F. M. *Phys. Rev. E* **1997**, *56* (1), 554.

(15) Jokisaari, J. In: *NMR of Ordered Liquids*; Burnell, E. E., de Lange, C. A., Eds.; Kluwer: Dordrecht, The Netherlands, 2003; p 109.

(16) Ylihautala, M.; Lounila, J.; Jokisaari, J. *J. Chem. Phys.* **1999**, *110*, 6381.

(17) de Gennes, P. G.; Prost, J. *The Physics of Liquid Crystals*, 2nd ed.; Clarendon Press: Oxford, U.K., 1998.

(18) Douglass, A. G.; Czuprynski, K.; Mierzwa, M.; Kaszynski, P. *J. Mater. Chem.* **1998**, *8* (11), 2391.

(19) Kralj, S.; Zidanšek, A.; Lahajnar, G.; Muševič, I.; Žumer, S.; Blinc, R.; Pintar, M. M. *Phys. Rev. E* **1996**, *53* (4), 3629.

(20) Abragam, A. *The Principles of Nuclear Magnetism*; Clarendon: Oxford, U.K., 1974.

(21) Jackson, C. L.; McKenna, G. B. *J. Chem. Phys.* **1990**, *93*, 9002.

(22) Van Geet, A. L. *Anal. Chem.* **1968**, *40*, 2227.

(23) Ratcliffe, C. I. *Annu. Rep. NMR Spectrosc.* **1998**, *36*, 124.

(24) Cook, G. A. *Argon, Helium and Rare Gases*; Interscience Publishers: New York, 1961.

(25) Telkki, V.-V.; Lounila, J.; Jokisaari, J. *J. Phys. Chem. B* **2005**, *109*, 757.

(26) Telkki, V.-V.; Lounila, J.; Jokisaari, J. *J. Phys. Chem. B,* **2005**, *109*, 24343.

(27) Telkki, V.-V.; Lounila, J.; Jokisaari, J. *J. Chem. Phys.* **2006**, *124*, 034711.

(28) Dunmur, D. A.; Fukuda, A.; Luckhurst, G. R. *Physical Properties of Liquid Crystals: Nematics*; INSPEC: London, 2001.

(29) Jameson, A. K.; Jameson, C. J.; Gutowsky, H. S. *J. Chem. Phys.* **1970**, *53*, 2310.

(30) Buckingham, A. D.; Burnell, E. D. *J. Am. Chem. Soc.* **1967**, *89*, 3341.

(31) Demus, D.; Goodby, J.; Gray, G. W.; Spiess, H.-W.; Vill, V. *Handbook of Liquid Crystals*; Wiley: Weinheim, Germany, 1998.

(32) Haller, I. *Prog. Solid State Chem.* **1975**, *10*, 103.

(33) Price, F. P.; Wendorff, J. H. *J. Phys. Chem.* **1972**, *76*, 2605.

(34) Bahadur, B.; Chandra, S. *J. Phys. C* **1976**, *9*, 5.

(35) Iannacchione, G. S.; Crawford, G. P.; Qian, S.; Doane, J. W.; Finotello, D.; Žumer, S. *Phys. Rev. E* **1996**, *53*, 2402

(36) Aksnes, D. W.; Førland, K.; Kimtys, L. *Phys. Chem. Chem. Phys.* **2001**, *3*, 3203.

(37) Aksnes, D. W.; Kimtys, L. *Appl. Magn. Reson.* **2002**, *23*, 51.

(38) Strange, J. H.; Rahman, M. *Phys. Rev. Lett.* **1993**, *71*, 3589.